


# Sol-gel synthesis and nonvolatile resistive switching behaviors of wurtzite phase ZnO nanofilms

Zhi-Qiang Yu(余志强), Jin-Hao Jia(贾金皓), Mei-Lian Ou(欧梅莲), Tang-You Sun(孙堂友), and Zhi-Mou Xu(徐智谋)

**Citation:**Chin. Phys. B, 2025, 34 (**12**): 127302. DOI: 10.1088/1674-1056/ade1c2
http://cpb.iphy.ac.cn; http://iopscience.iop.org/cpb

**What follows is a list of articles you may be interested in**

---

## A universal resist-assisted metal transfer method for 2D semiconductor contacts

Xuanye Liu(刘轩冶), Linxuan Li(李林璇), Chijun Wei(尉驰俊), Peng Song(宋鹏), Hui Gao(高辉), Kang Wu(吴康), Nuertai Jiazila(努尔泰·加孜拉), Jiequn Sun(孙杰群), Hui Guo(郭辉), Haitao Yang(杨海涛), Wu Zhou(周武), Lihong Bao(鲍丽宏), and Hong-Jun Gao(高鸿钧)

Chin. Phys. B, 2024, 33 (**12**): 127302. DOI: 10.1088/1674-1056/ad8db4

## Exploring reservoir computing: Implementation via double stochastic nanowire networks

Jian-Feng Tang(唐健峰), Lei Xia(夏磊), Guang-Li Li(李广隶), Jun Fu(付军), Shukai Duan(段书凯), and Lidan Wang(王丽丹)

Chin. Phys. B, 2024, 33 (**3**): 037302. DOI: 10.1088/1674-1056/aceeea

## Simulation of optical and electrical synaptic functions in $MoS_2/\alpha$-$In_2Se_3$ heterojunction memtransistors

Tao Xiang(相韬), Fengxiang Chen(陈凤翔), Xiaoli Li(李晓莉),Xiaodong Wang(王小东), Yuling Yan(闫誉玲), and Lisheng Wang(汪礼胜)

Chin. Phys. B, 2023, 32 (**11**): 117301. DOI: 10.1088/1674-1056/acee58

## Epitaxial $Bi_2Sr_2CuOy$ thin films as p-type transparent conductors

Chen Zhou(周臣), Wang-Ping Cheng(程王平), Yuan-Di He(何媛娣), Cheng Shao(邵成), Ling Hu(胡令), Ren-Huai Wei(魏仁怀), Jing-Gang Qin(秦经刚), Wen-Hai Song(宋文海), Xue-Bin Zhu(朱雪斌), Chuan-Bing Cai(蔡传兵), and Yu-Ping Sun(孙玉平)

Chin. Phys. B, 2022, 31 (**10**): 107305. DOI: 10.1088/1674-1056/ac67ca

## Digital and analog memory devices based on 2D layered $MPS_3$ ( $M$=Mn, Co, Ni) materials

Guihua Zhao(赵贵华), Li Wang(王力), Xi Ke(柯曦), and Zhiyi Yu(虞志益)

Chin. Phys. B, 2021, 30 (**4**): 047303. DOI: 10.1088/1674-1056/abd397

---

# Sol–gel synthesis and nonvolatile resistive switching behaviors of wurtzite phase ZnO nanofilms

Zhi-Qiang Yu(余志强)[1,2,4,†], Jin-Hao Jia(贾金皓)[1], Mei-Lian Ou(欧梅莲)[1], Tang-You Sun(孙堂友)[3,4,‡], and Zhi-Mou Xu(徐智谋)[4]

[1] *School of Electronic Engineering, Guangxi University of Science and Technology, Liuzhou* 545006, *China*
[2] *School of Computer and Information Technology, Hohhot Minzu College, Hohhot* 010051, *China*
[3] *Guangxi Key Laboratory of Precision Navigation Technology and Application, Guilin University of Electronic Technology, Guilin* 541004, *China*
[4] *Wuhan National Laboratory for Optoelectronics, School of Optical and Electronic Information, Huazhong University of Science and Technology, Wuhan* 430074, *China*

(Received 10 April 2025; revised manuscript received 11 May 2025; accepted manuscript online 6 June 2025)

A facile sol–gel method and heating treatment process have been reported to synthesize the wurtzite phase ZnO nanofilms with the preferential growth orientation along the [001] direction on the FTO substrates. The as-prepared wurtzite phase ZnO nanofilms-based memristor with the W/ZnO/FTO sandwich has demonstrated a reliable nonvolatile bipolar resistive switching behaviors with an ultralow set voltage of about +3 V and reset voltage of approximately −3.6 V, high resistive switching ratio of more than two orders of magnitude, good resistance retention ability (up to $10^4$ s), and excellent durability. Furthermore, the resistive switching behavior in the low-resistance state is attributed to the Ohmic conduction mechanism, while the resistive switching behavior in the high-resistance state is controlled by the trap-modulated space charge limited current (SCLC) mechanism. In addition, the conductive filament model regulated by the oxygen vacancies has been proposed, where the nonvolatile bipolar resistive switching behaviors could be attributed to the formation and rupture of conductive filaments in the W/ZnO/FTO memristor. This work demonstrates that the as-prepared wurtzite phase ZnO nanofilms-based W/ZnO/FTO memristor has promising prospects in future nonvolatile memory applications.

**Keywords:** sol–gel, ZnO nanofilms, memristor, nonvolatile, oxygen vacancies

**PACS:** 73.40.Rw, 72.60.+g, 72.80.Ga

**DOI:** 10.1088/1674-1056/ade1c2 **CSTR:** 32038.14.CPB.ade1c2

## 1. Introduction

Resistive random access memory (ReRAM) is a new type of nanodevice that is becoming a research hotspot for next-generation nonvolatile storage devices due to its excellent durability, ultra-low power consumption, fast storage speed, and ultra-high storage density.[1–3] This device represents the fourth type of circuit element: the memristor.[4] Compared to thin films, the practical application of memristors has structural advantages by introducing nanofilms into ReRAM devices, which is expected to improve the performance of memory devices. For example, during the operation of the resistive switch, the presence of the nanofilm will promote the formation of linear conduction paths, thereby enhancing the transport of charge carriers. This stands in stark contrast to the branched conductive wires commonly found in the internal structure of film-based materials. Therefore, the presence of the nanofilm can achieve high-quality memristor performance, as well as good stability and repeatability.

In recent years, various transition metal oxides, such as ZnO,[5–9] $TiO_2$,[10–13] $HfO_2$,[14] $Al_2O_3$,[15] $SnO_2$,[16] $Fe_2O_3$,[17] $ZrO_2$,[18] NiO,[19] $WO_3$,[20] $PbTiO_3$,[21] and $BiFeO_3$[22] have been developed for use in ReRAM resistive switching layers due to their unique resistive switching behavior. ZnO, as a third-generation semiconductor, is a wide-bandgap direct bandgap semiconductor material with a bandwidth of approximately 3.37 eV. It has a series of advantages, such as high temperature resistance (1975 °C), multi-process preparation, and low toxicity, making it widely applicable in fields like space technology, optoelectronics, and high-density information storage. Recently, various approaches have been developed to fully realize the potential applications of ZnO, including the metal chemical vapor deposition (MOCVD),[23] pulsed laser deposition (PLD), hydrothermal method,[24] magnetron sputtering,[25] atomic layer deposition (ALD), molecular beam epitaxy (MBE), and sol–gel method. Among them, the sol–gel method has demonstrated the advantages of low cost, simple setup, low power dissipation, and relatively mild reaction conditions, which offers a high-efficiency approach for the controlled large-scale synthesis of the ZnO nanofilms. It has been widely adopted to prepare the various ZnO nanofilms-based devices. Sun *et al.*[26] synthesized the ZnO nanorods (ZnO NRs) using rapid hydrogen annealing technology. Based on this nanodevice, a memristor with

†Corresponding author. E-mail: zhiqiangyu@alumni.hust.edu.cn
‡Corresponding author. E-mail: suntangyou@guet.edu.cn

© 2025 Chinese Physical Society and IOP Publishing Ltd. All rights, including for text and data mining, AI training, and similar technologies, are reserved.

an Au/ZnO NRs/AZO (Al-doped ZnO conductive glass) MIM structure was fabricated. Although the performance of this equipment is quite impressive, the cost of using this method to prepare nanomaterials is relatively high, making it unsuitable for large-scale production. Xu *et al.*[27] obtained the ZnO nanofilms through pulsed laser deposition and prepared the Pt/ZnO/Pt/STO resistive switching devices with a heterostructure. However, the performance of these devices is not very outstanding, and this preparation method requires prolonged combustion under high-temperature conditions. This process is complex and costly, making large-scale production difficult and hindering the market application of resistive random-access memory (ReRAM). Karthik *et al.*[28] synthesized the ZnO nanowires (ZnO NWs) using metal chemical vapor deposition technology to create a memristor with a Pt/ZnO NWs/Pt structure. This preparation method has strict reaction conditions; the vapors of many metal compounds are harmful to the human body. Moreover, the performance of this device is not outstanding, so this method is not suitable for practical applications. Quan *et al.*[29] used the tea leaves as materials and a green process to synthesize the ZnO nanoparticles (ZnO NPs) and prepared an Ag/ZnO NPs/ITO structure memristor. However, the performance of these devices is not outstanding. Summarizing previous work, although ZnO nanomaterial memristors have broad application prospects in the next generation of nonvolatile advanced memory, there are still some shortcomings in the preparation of resistive memory materials, the On/Off ratio of memristors, and the ZnO nanofilms used for ReRAM. Additionally, the resistive switching mechanism in the ZnO nanofilms-based device prepared by the sol–gel process is still mysterious.

Herein, a facile and efficient sol–gel spin-coating process was used to synthesize the wurtzite phase ZnO nanofilms on the FTO substrates, achieving stable nonvolatile and unformed bipolar resistive switching behaviors in the ZnO nanofilms-based W/ZnO/FTO memristor. Moreover, the redistribution of the conductive filament regulated by the oxygen vacancies in the as-prepared wurtzite phase ZnO nanofilms has been suggested to be responsible for the nonvolatile resistive switching behaviors in the ZnO nanofilms-based W/ZnO/FTO memristor.

## 2. Experimental details

For the ZnO nanofilms-based memristor with the W/ZnO/FTO sandwich, the resistive switching material ZnO nanofilms have been prepared by a facile and efficient sol–gel spin-coating process. During the spin-coating preparation of ZnO nanofilms, all the chemical reagents used were of analytical grade and purchased from Aladdin Reagents Company. No further purification treatment was conducted before use; the substrate FTO (fluorine-doped tin oxide, 6.3 Ω/square) was also commercially purchased from Hartford Glass Company. First, dissolve the 0.015-M zinc acetate dihydrate ($Zn(C_2H_3O_2)_2{\cdot}2H_2O$, 99%) crystals in a mixture containing 20 mL of ethylene glycol methyl ether ($C_3H_8O_2$,99.7%) and 600 μL of ethanolamine ($NH_2(CH_2)_2ON$, 99%). Stir continuously at 1200 rpm for 3 hours at 60 °C to obtain a transparent precursor solution, which serves as the ZnO precursor solution. After cleaning the FTO substrate with deionized water, anhydrous ethanol, and acetone in a 1:1:1 ratio and sonicate for 10 min, and then dry in an oven. Use a pipette to transfer 100 μL of precursor solution dropwise onto a fixed FTO glass slide. Start the spin coater (Coater, KW-4T Institute of Microelectronics, Chinese Academy of Sciences, China); first spin at 1000 rpm for 10 s to make it uniform, then spin at 3500 rpm for 30 s to form a uniform ZnO precursor film. Place the spin-coated film sample on the heating plate and dry it at 60 °C for 5 min to complete the leveling step. Repeat the above steps 10 times and place the sample into a preheated muffle furnace at 800 °C for 20 min and then allow it to cool naturally to room temperature to obtain the dense and orderly ZnO nanofilms. The preparation process of the ZnO nanofilms has been shown in Fig. 1.

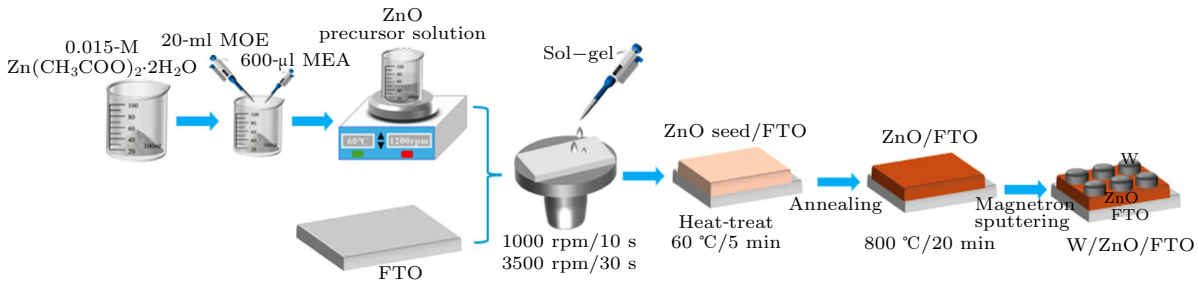



**Fig. 1.** Preparation process of the ZnO nanofilms.

To test the electrical performance of the sample, the tungsten wafer array with a diameter of approximately 5 μm was deposited on the surface of the ZnO nanofilms using magnetron sputtering technology after the oxide nanofilms had been cured and formed. As the top electrode of the ZnO nanofilms memristor structure, the W/Zeno/FTO memristor with a metal/resistive layer/metal (M/I/M) structure was obtained, as shown in Fig. 2. Apply cyclic scan voltage to

the upper electrode, ground the lower electrode, and test the electrical characteristics of the device; use scanning electron microscopy (SEM, FEI Nova NanoSEM 450, Lincoln, UN, USA) to characterize the morphology of the ZnO film and examine the quality of the ZnO nanofilms; use x-ray diffraction (XRD, PANalytical PW3040/60 Spectris UK) and x-ray photoelectron spectroscopy (XPS, AXIS-ULTRA DLD-600W Shimadzu-Kratos Japan) to analyze the crystal structure and composition of the ZnO nanofilms.

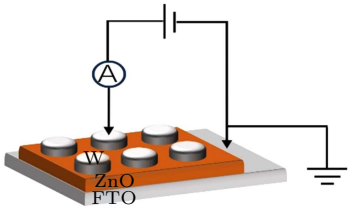



**Fig. 2.** Schematic model of the as-prepared W/ZnO/FTO memristor.

## 3. Results and discussion

Figure 3(a) shows the XRD patterns of ZnO nanofilms prepared by a simple sol–gel spin-coating method. From the XRD patterns, the diffraction peak corresponding to the (002) plane of the as-prepared ZnO nanofilms sample is significantly enhanced. The presence of strong peak in the XRD patterns indicates that the crystal quality of the ZnO nanofilms is good, and the ZnO nanofilms prepared by the sol–gel spin-coating process primarily grow along the [001] direction, which are classified as the wurtzite phase (JCPDS Card No. 36-1451).[7,30] Figures 3(b) and 3(c) are the top-view FESEM images of the as-prepared ZnO nanofilms under different magnifications. It can be intuitively observed that the surface morphology of the ZnO nanofilms is dense, orderly, and neat; the ZnO nanocrystals grow well and are evenly distributed. The as-prepared ZnO nanocrystals are arranged in an orderly and dense manner, uniformly and roughly in a hexagonal structure, which is consistent with the structural characteristics of the wurtzite phase ZnO. In addition, the entire surface of the as-prepared ZnO nanofilms is relatively uniform, which is comprised of the ZnO nanograins with an average size of 25.5 nm, as shown in the inset of Fig. 3(c). Figure 3(d) is the FESEM image of the cross-sectional morphology of the ZnO nanofilms. The results indicate that the ZnO nanofilms prepared by the sol–gel spin-coating process have a thickness of approximately 100 nm, which can serve as the resistive switching layer of the as-prepared wurtzite phase ZnO nanofilms-based W/ZnO/FTO memristor.

To confirm the surface composition and chemical state of the prepared ZnO nanofilms, XPS spectroscopy was used to analyze the chemical bonding states of the elements in the ZnO nanofilms. XPS spectroscopy is commonly used to study the surface chemical analysis of ZnO nanofilms. Figure 4(a) shows the XPS spectrum of the ZnO film, indicating that the prepared ZnO film contains only three elements: Zn, O, and C. The reason for the small carbon peak is the carbon source in the air, which adsorbs onto the surface of the prepared ZnO nanofilms and is used to calibrate the effects of other elements, including Zn and O. Figure 4(b) shows the high-resolution Zn 2p XPS spectrum of the ZnO nanofilms and the corresponding Gaussian fitting peaks. It can be clearly seen that, from left to right, there are two peaks in the Zn 2p XPS spectrum, with binding energies of 1021.23 eV and 1044.29 eV, respectively. The reason for the Zn 2p XPS peak is that the binding energy of Zn $2p_{3/2}$ is 1021.23 eV, and the binding energy of Zn $2p_{1/2}$ is 1044.29 eV. The spin–orbit coupling energy between Zn $2p_{1/2}$ and Zn $2p_{3/2}$ is estimated to be 23.06 eV, indicating the presence of $Zn^{2+}$ in the ZnO nanofilms. Figure 4(c) shows the high-resolution O 1s XPS spectrum of the prepared ZnO nanofilms. The results indicate that the O 1s XPS spectrum of the ZnO nanofilms can be deconvoluted into three Gaussian fitting peaks, located at three binding energies: 529.82 eV, 530.66 eV, and 531.70 eV. This phenomenon can be attributed to the binding of oxygen ions with the ZnO nanofilms at 529.82 eV; at 530.66 eV, the presence of many oxygen vacancies and the Gaussian peak at 531.70 eV are due to some oxygen molecules adhering to the surface of the ZnO nanofilms. The fitting results of the asymmetric O 1s XPS spectrum indicate that there are many oxygen vacancies in the ZnO nanofilms prepared by the sol–gel spin-coating method.[24] This means that these oxygen vacancies can act as charge carriers and electron traps in the W/ZnO/FTO memristor, resulting in the W/ZnO/FTO memristor exhibiting nonvolatile resistive switching characteristics.

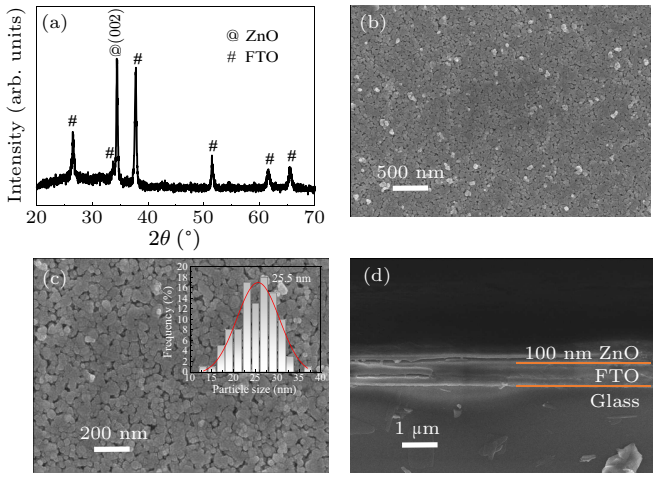



**Fig. 3.** (a) XRD patterns of the ZnO nanofilms. (b) and (c) Top view of FESEM for the ZnO nanofilms under different magnifications, the inset of (c) is the size distribution histogram of the ZnO nanograins, (d) FESEM cross-sectional images of the ZnO nanofilms.

To illustrate the nonvolatile resistive switching performance of W/ZnO/FTO memristor prepared by the sol–gel spin-coating method with ZnO nanofilm structure, typical *I*–*V* measurements were conducted on W/ZnO/FTO memristor

with ZnO nanofilm structure. The cyclic scan voltage is applied in the order of 0 V $\rightarrow$ +3 V $\rightarrow$ 0 V $\rightarrow$ −4 V $\rightarrow$ 0 V, with a fixed current limit of 3 mA. The purpose of setting a current limit is to protect the equipment from irreversible damage during testing, as shown in Fig. 5. Figure 5(a) shows the linear *I*–*V* curve of the W/ZnO/FTO memristor device after 100 consecutive cycles. The arrows and numbers in the diagram represent the scanning direction and sequence of the device bias voltage, respectively. Figure 5(b) shows the *I*–*V* curve of the W/ZnO/FTO memristor device in semi-logarithmic coordinates after 100 consecutive cycles. The W/ZnO/FTO memristor with a ZnO nanofilm structure exhibits stable nonvolatile bipolar resistive switching performance. The initial resistance state of the W/ZnO/FTO memristor is HRS. When the cyclic scan voltage increases from 0 V to +3 V, the W/ZnO/FTO memristor device will transition from HRS to LRS, completing the set process at approximately +3 V. Subsequently, the W/ZnO/FTO memristor will maintain LRS until the reverse voltage drops to −3.6 V, at which point the W/ZnO/FTO memristor will return to HRS, demonstrating the nonvolatile bipolar resistive switching behaviors of the W/ZnO/FTO memristor.

To further illustrate the resistive switching mechanism of the W/ZnO/FTO memristor, we plotted the *I*–*V* curves of the device on a logarithmic scale, as shown in Figs. 5(c) and 5(d). Figure 5(c) shows the double logarithmic *I*–*V* curve of the W/ZnO/FTO memristor within the positive voltage range. In the LRS, the slope of the linear *I*–*V* curve in the LRS region is approximately 1.30, indicating that the device follows an ohmic conduction mechanism ($I \propto V$). In the HRS region, as the positive voltage increases, the slope of the *I*–*V* curve varies between 1.28 and 2.81 and then reaches 3.81. The complex *I*–*V* curve in HRS can be decomposed into two distinct regions, corresponding to the Child's law region ($I \propto V^2$) and the trap-filled limit region ($I \propto V^m$, $m > 2$), indicating that the device in HRS follows the SCLC controlled by the oxygen vacancy related traps.[31] In the LRS, thermally generated carriers dominate the conductive behavior, and the device exhibits a linear Ohmic conduction mechanism in the HRS. As the positive voltage increases, the injected carriers gradually occupy and dominate the capture centers composed of oxygen vacancies. The resistance switching behavior of W/ZnO/FTO memristor sequentially follows Child's law and the trap-filled limited conduction mechanism. Afterwards, a setting process occurs at $V_{set}$, and the device switches to LRS, resulting in an increase in current, indicating the formation of oxygen vacancies conductive nanowires. Figure 5(d) shows the double logarithmic *I*–*V* curve of the W/ZnO/FTO memristor in the negative voltage region. Compared to the positive voltage region, the device has a similar resistance switching mechanism in the negative voltage region. The slope of the linear *I*–*V* curve is 1.09, revealing the ohmic conduction mechanism of the device in the LRS region. As the negative voltage increases, the device will maintain LRS until a sufficiently large negative cycling voltage is applied until $V_{reset}$. Afterwards, a reset process occurs at $V_{reset}$. As the current decreases, the device transitions from LRS to HRS, indicating the rupture of the oxygen vacancy-based conductive filament. Subsequently, as the negative voltage in the HRS region decreases, the slope of the *I*–*V* curve changes from 3.96 to 2.6 and then to 1.15, which also demonstrates the presence of a trap-controlled space charge-limited current mechanism in the HRS region of the as-prepared wurtzite phase ZnO nanofilms-based W/ZnO/FTO memristor.

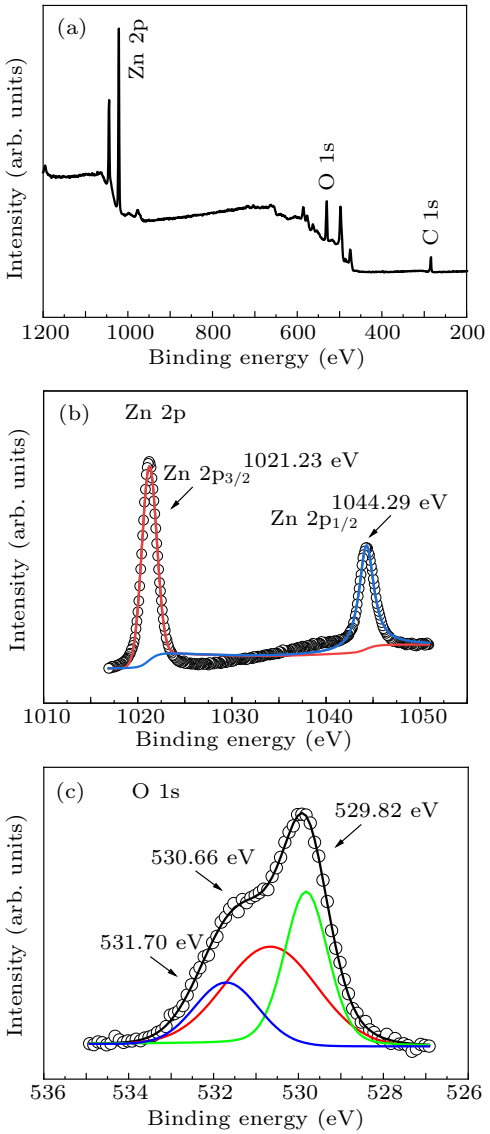



**Fig. 4.** (a) XPS survey spectrum of the as-prepared ZnO nanofilms. (b) Zn 2p, and (c) O 1s high-resolution XPS spectra, respectively.

In the Ohmic region, the expression for calculating the current density $J_0$ can be expressed as[10–13]

$$J_0 = qn\mu\frac{V}{d}, \tag{1}$$

where $q$ is the basic charge, $n$ is the density of free charge carriers generated by heat, $\mu$ is the electron mobility, $V$ is the

applied scanning voltage, and $d$ is the thickness of the ZnO layer in the ZnO nanofilms-based W/ZnO/FTO memristor.

In the high resistance conduction region, the current density $J_c$ can be given as

$$J_c = \frac{9}{8}\varepsilon\mu\xi\frac{V^2}{d^3}, \tag{2}$$

where $\varepsilon$ is the dielectric constant of the ZnO resistive layer, and $\xi$ is the ratio of the free carrier density to the total carrier density. Clearly, the resistance change behavior of the as-prepared W/ZnO/FTO memristor transitions from a high resistance state to a low resistance state during the set process and then returns to HRS during the reset process, which may correspond to the formation and rupture of oxygen vacancies conductive channels, respectively. Therefore, the nonvolatile bipolar resistive behavior of W/ZnO/FTO memristor can be explained by the formation and rupture of conductive filaments induced by oxygen vacancy migration under external bias voltage, which is the resistance switching mechanism.

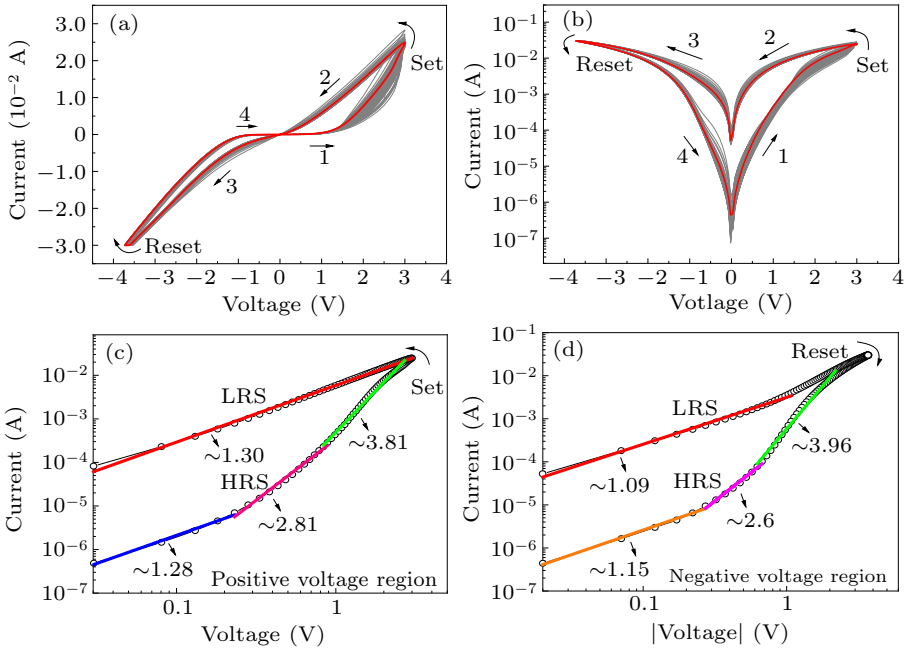



**Fig. 5.** Electrical characteristics of the W/ZnO/FTO memristor. (a) Linear $I$–$V$ curve after 100 consecutive cycles, (b) semi-logarithmic $I$–$V$ curve after 100 consecutive cycles. Double logarithmic $I$–$V$ curves in the positive voltage region (c) and in the negative voltage region (d).

The electrochemical reaction process for generating oxygen vacancies in the as-prepared wurtzite phase ZnO nanofilms-based W/ZnO/FTO memristor can be described as:[10] $O_0^x \rightarrow V_{\ddot{O}} + O^{2-}$, where $O_0^x$ is the oxygen atom at the normal lattice position in the ZnO nanofilm resistance layer, $O^{2-}$ is the oxygen ion with two negative charges, and $V_{\ddot{O}}$ is an oxygen vacancy that has lost an electron and carries a positive charge. As the forward scan voltage increases, the oxygen vacancies move towards the lower electrode of the FTO under the excitation of the external electric field. The oxygen ions will be adsorbed near the W electrode, forming a conductive filament composed of oxygen vacancies defects within the resistance layer of the device. As the forward scanning voltage of the device gradually increases, when the voltage reaches the set voltage, conductive filaments of oxygen vacancies have already formed inside the device, at which point the device transitions from a high resistance state to a low resistance state. When a reverse scan voltage is applied to the W/ZnO/FTO memristor, the oxygen vacancies in the internal resistive storage layer of the device move towards the W top electrode under the excitation of the external electric field. The oxygen ions adsorbed near the W electrode will also be released and undergo a reset reaction with the oxygen vacancies. The electrochemical reaction process is as follows: $V_{\ddot{O}} + O^{2-} \rightarrow O_0^x$. At this point, the conductive filaments based on oxygen vacancies begin to break. When the reverse scan voltage of the device drops to the reset voltage, the conductive filaments inside the resistive storage layer completely break, and the W/ZnO/FTO memristor transitions from LRS to the HRS.

To evaluate the potential in nonvolatile memory applications of the W/ZnO/FTO memristor. The retention and endurance capabilities between HRS and LRS at the read voltage of 0.5 V for the W/ZnO/FTO memristor has been demonstrated, as shown in Fig. 6. The resistive switching ratio between the HRS and LRS exceeds two orders of magnitude and can be stably remained over $10^4$ s, showing no significant decline. At the same time, compared with the previous literatures[32–34,36–38,42,44,46] about the ZnO-based memristors, the resistive switching ratio of the as-prepared W/ZnO/FTO memristor in this work has increased by at least one order of magnitude, demonstrating the superior nonvolatile memory

performance of the W/ZnO/FTO memristor.

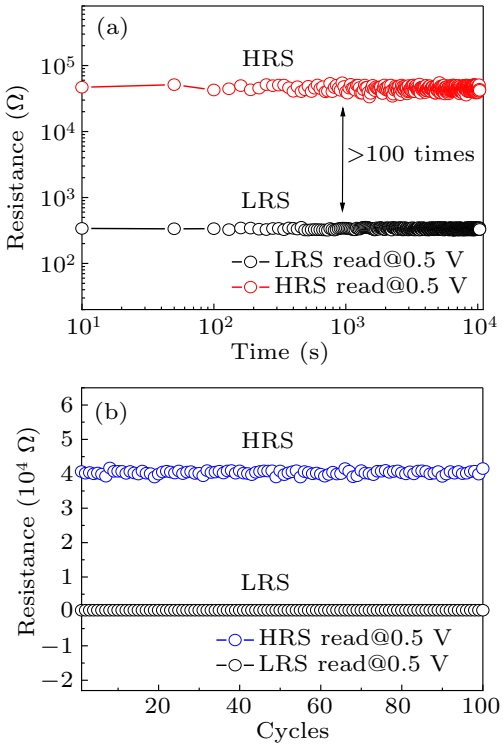



**Fig. 6.** (a) Retention and (b) endurance capabilities between HRS and LRS at the read voltage of 0.5 V for the as-prepared W/ZnO/FTO memristor.

To further estimate the overall performances of the the as-prepared ZnO nanofilms-based W/ZnO/FTO memristor, Table 1 presents a comparison of the memristor's performances with the previous literatures about the ZnO-based memristors.[32–46] It is obvious that the as-prepared W/ZnO/FTO memristor in this work has demonstrated the nonvolatile bipolar resistive switching behaviors with a lower set voltage of about +3 V and reset voltage of approximately −3.6 V, high resistive switching ratio of larger than two orders of magnitude, and good resistive switching retention capability (up to $10^4$ s), suggesting that the W/ZnO/FTO memristor has the promising prospects in future nonvolatile memory applications.

The conductive filament model regulated by the oxygen vacancies can be used to explain the resistive switching behavior of the ZnO nanofilms-based resistive memory devices, and the intrinsic defects have been formed in ZnO nanofilms during the annealing process. These defects may include oxygen vacancies, interstitial atoms, or other defects, but oxygen vacancies are considered the most important. The switching mechanism of the conductive wire is shown in Fig. 7. As the upper electrode, it is known that the W electrode plays an important electrochemical role in the formation and rupture of conductive wires. When a positive voltage is applied to the upper electrode relative to the lower FTO electrode, W is oxidized, and these cations are reduced at the bottom FTO electrode through the active ZnO layer. The precipitation of W metal atoms at the bottom of the FTO electrode leads to the growth of W wires in the ZnO layer. As shown in Fig. 7, the metal wire is ultimately connected to the upper electrode. Fully grown conductive filaments help switch the device to the LRS state. In the next case, due to the change in the polarity of the applied voltage, W underwent electrochemical dissolution. The change in polarity caused the conductive wire to break, putting the device into HRS mode. In short, the redistribution of the conductive filament regulated by the oxygen vacancies may be the main reason for the nonvolatile bipolar resistive switching behaviors in the W/ZnO/FTO memristor.

**Table 1.** Comparison of the performances for the ZnO-based memristors.

| Device Structure | $V_{reset}/V_{set}$ (V) | Preparation process | $R_{HRS}/R_{LRS}$ ratio | Retention (s) | Endurance (cycles) | Reference |
|---|---|---|---|---|---|---|
| Al/ZnO/Al | −6.2/6.3 | dual ion beam sputtering | ∼ 10 | $10^6$ | 250 | [32] |
| Cu/Fe@ZnO/Zn | −6/6 | hydrothermal | ∼ 1.81 | – | 5 | [33] |
| Al/ZnO/Al | ∼ −2/ ∼ 1.5 | magnetron sputtering | 10 | – | 100 | [34] |
| Pt/$TiO_x$/ZnO/$SiO_2$/TaN | −2/5 | ALD | ∼ 102 | $10^4$ | 150 | [35] |
| Pt/ZnO/Fe/ZnO/ITO | ∼ −6/ ∼ 5 | RF/DC magnetron sputtering | ∼ 6 | $4 \times 10^4$ | – | [36] |
| Pt/ZnO-graphene/Pt | −5/+5 | CVD | ∼ 7.12 | – | – | [37] |
| Au/ZnO/Au | −6/+6 | di electrophoresis | ∼ 10 | 60 | 10 | [38] |
| GZO/$ZnO_2$/ZnO/ITO | ∼ −3/ ∼ +7 | magnetron sputtering | ∼ 102 | | 10 | [39] |
| AZO/ZnO/ITO | −5/+5 | magnetron sputtering | ∼ 102 | | 100 | [40] |
| Au/Co-ZnO/Au/$SiO_2$ | −4.5/3.5 | hydrothermal | ∼ 50 | $10^3$ | 100 | [41] |
| Pt/ZnO/Pt/Ti/$SiO_2$/Si | ∼ −2/ ∼ +2 | magnetron sputtering | ∼ 10 | $10^4$ | 100 | [42] |
| Pt/ZnO/Pt | −1.5/+2 | magnetron sputtering | ∼ 102 | $10^4$ | 500 | [43] |
| AZO/ZnO/$TiO_2$/$Al_2O_3$/AZO | ∼ −15/ ∼ +15 | ALD | ∼ 10 | – | 100 | [44] |
| TiN/ZnO/W | −2/+2 | pulsed laser deposition | ∼ 102 | | 300 | [45] |
| Ag/ZnO/$WO_x$/FTO | ∼ −4/ ∼ +4 | magnetron sputtering | ∼ 11.7 | $10^4$ | – | [46] |
| W/ZnO/FTO | −3.6/+3 | spin coating technique | $> 10^2$ | $\sim 10^4$ | > 100 | this work |

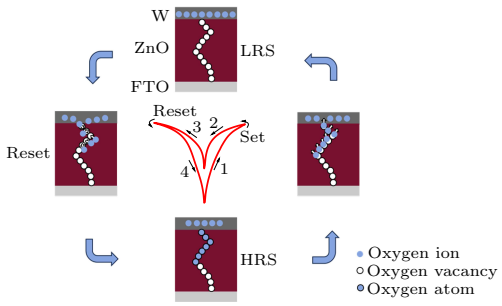



**Fig. 7.** Schematic diagram of the resistive switching mechanism for the W/ZnO/FTO memristor.

## 4. Conclusion

To summarize, this paper has demonstrated a facile sol–gel method and heating treatment process to prepare the wurtzite phase ZnO nanofilms with the preferential growth along the [001] direction on FTO substrate. The as-prepared wurtzite phase ZnO nanofilms-based W/ZnO/FTO memristor with a sandwich structure exhibits a reliable nonvolatile bipolar resistive switching characteristic. High resistive switching ratio of more than two orders of magnitude, good resistance retention ability (up to $10^4$ s), low set voltage of about $+3$ V and reset voltage of approximately $-3.6$ V, and excellent durability have been obtained in the as-prepared wurtzite phase ZnO nanofilms-based W/ZnO/FTO memristor. The nonvolatile bipolar resistive switching behaviors of the W/ZnO/FTO memristor have been elucidated by the redistribution of the conductive filament regulated by the oxygen vacancies. This work has demonstrated that the as-prepared wurtzite phase ZnO nanofilms-based memristor is a promising candidate for future nonvolatile memory applications.

## Acknowledgements

Project supported by the National Natural Science Foundation of China (Grant Nos. 62341305, 61805053, and 22269002) and the Science and Technology Project of Guangxi Zhuang Autonomous Region, China (Grant Nos. AD19110038 and AD21238033). The authors would like to thank the Shiyanjia (www.shiyanjia.com) for the XPS test and XRD refinement.

## References

[1] Persson K M, Ram M S, Kilpi O P, Borg M and Wernersson L E 2020 *Adv. Electron. Mater.* **6** 2000154
[2] Alagoz H S, Chow K H and Jung J 2019 *Appl. Phys. Lett.* **114** 163502
[3] Manning H G, Biswas S, Holmes J D and Boland J J 2017 *ACS Appl. Mater. Interfaces* **9** 38959
[4] Chua L 1971 *IEEE Transactions on Circuit Theory* **18** 507
[5] Qiao Y, Chen J Q, Zhou S S, Chen J G, Jiang S C and Yang Y J 2024 *Chin. Phys. Lett.* **41** 014205
[6] Milano G, Luebben M, Ma Z, Dunin-Borkowski R, Boarino L, Pirri C F, Waser R, Ricciardi C and Valov I 2018 *Nat. Commun.* **9** 5151
[7] Sarkar D and Singh A K 2017 *J. Phys. Chem. C* **121** 12953
[8] Khan M U, Hassan G and Bae J 2020 *Journal of Materials Science: Materials in Electronics* **31** 1105
[9] Qi M, Zhang X, Yang L, Wang Z Q, Xu H Y, Liu W Z, Zhao X N and Liu Y C 2018 *Appl. Phys. Lett.* **113** 223503
[10] Yu Z Q, Liu M L, Lang J X, Qian K and Zhang C H 2018 *Acta Phys. Sin.* **67** 157302 (in Chinese)
[11] Yu Z Q, Sun T Y, Liu B S, Zhang L, Chen H J, Fan X S and Sun Z J 2021 *J. Alloys Compd.* **858** 157749
[12] Yu Z Q, Qu X P, Yang W P, Peng J and Xu Z M 2016 *J. Alloys Compd.* **688** 37
[13] Yu Z Q, Qu X P, Yang W P, Peng J and Xu Z M 2016 *J. Alloys Compd.* **688** 294
[14] Chen Q L, Liu G, Xue W H, Shang J, Gao S, Yi X H, Lu Y, Chen X H, Tang M H, Zheng X J and Li R W 2019 *ACS Appl. Electron. Mater.* **1** 789
[15] Kim S M, Kim H J, Jung H J, Kim S H, Park J Y, Seok T J, Park T J and Lee S W 2019 *ACS Appl. Mater. Interfaces* **11** 30028
[16] Wu X H, Xu Z Q, Yu Z M, Zhang T, Zhao F, Sun T Y, Ma Z C, Li Z P and Wang S B 2015 *J. Phys. D: Appl. Phys.* **48** 115101
[17] Yu Z Q, Xu J M, Liu B S, Sun Z J, Huang Q N, Ou M L, Wang Q C, Jia J H, Kang W B, Xiao Q Q, Gao T H and Xie Q 2023 *Molecules* **28** 3835
[18] Hsu C C, Wang T C and Tsao C C 2018 *J. Alloys Compd.* **769** 65
[19] You B K, Park W I, Kim J M, Park K, Seo H K, Lee J Y, Jung Y S and Lee K J 2014 *ACS Nano* **8** 9492
[20] Zhao G, Yin Y L, Peng Y H, Yang W J, Liu Y H, Wang W K, Zhou W C and Tang D S 2019 *J. Appl. Phys.* **126** 54303
[21] Song W B, Xi G Q, Pan Z, Liu J, Ye X B, Liu Z H, Wang X, Shan P F, Zhang L X, Lu N P, Fan L L, Qin X M and Long Y W 2024 *Chin. Phys. B* **33** 057701
[22] Sharon V S, Veena Gopalan E and Malini K A 2023 *Chin. Phys. B* **32** 037504
[23] Huang C H, Huang J S, Lin S M, Chang W Y, He J H and Chueh Y L 2012 *ACS Nano* **6** 8407
[24] Tang J, Chai J W, Huang J, Deng L Y, Nguyen X S, Sun L F, Venkatesan T, Shen Z X, Tay C B and Chua S J 2015 *ACS Appl. Mater. Interfaces* **7** 4737
[25] Wang H J, Zhu Y Y and Liu Y 2018 *Chin. J. Phys.* **56** 3073
[26] Sun Y H, Yan X Q, Zheng X, Liu Y C, Zhao Y G, Shen Y W, Liao Q L and Zhang Y 2015 *ACS Appl. Mater. Interfaces* **7** 7382
[27] Xu J, Shang Z X, Hou Z P and Wang X L 2022 *Surfaces and Interfaces* **31** 102014
[28] Karthik K R G, Prabhakar R R, Hai L, Batabyal S K, Huang Y Z and Mhaisalkar S G 2013 *Appl. Phys. Lett.* **103** 123114
[29] Pham Q P, Nguyen Q N L, Nguyen N H, Doan U T T, Ung T D T, Tran V C, Phan T B, Pham A T T and Pham N K 2023 *Ceramics International* **49** 20742
[30] Li S Q, Lv J G, Lu B J, Yang R Q, Lu Y D, Wang F Z and Ye Z Z 2023 *J. Mater. Sci. Eng.* **41** 532
[31] Hsu C C, Wang S Y, Lin Y S and Chen Y T 2019 *J. Alloys Compd.* **779** 609
[32] Kumar A, Das M, Garg V, Sengar B S, Htay M T, Kumar S, Kranti A and Mukherjee S 2017 *Appl. Phys. Lett.* **110** 253509
[33] Wang J, Pei X Y, Zhang J W, Li Y, Chen J B and Wang C W 2022 *Ceramics International* **48** 15824
[34] Gul F and Efeoglu H 2017 *Superlattices and Microstructures* **101** 172
[35] Ismail M, Rasheed M, Mahata C, Kang M G and Kim S J 2023 *J. Alloys Compd.* **960** 170846
[36] Santos Y P, Valença E, Machado R and Macêdo M A 2018 *Mater. Sci. Semicond. Process.* **86** 43
[37] Aziz T N T Z, Rosli A B, Yusoff M M, Herman S H and Zulkifli Z 2019 *Mater. Sci. Semicond. Process.* **89** 68
[38] Zhao B, Xiao M, Shen D Z and Zhou Y N 2020 *Nanotechnology* **31** 125201
[39] Simanjuntak F M, Chandrasekaran S, Lin C C and Tseng T Y 2019 *APL Mater.* **7** 051108
[40] Simanjuntak F M, Ohno T and Samukawa S 2019 *AIP Adv.* **9** 105216
[41] Elboughdiri N, Iqbal S, Abdullaev S, Aljohani M, Safeen A, Althubeiti K and Khan R 2023 *RSC Adv.* **13** 35993
[42] Huang C H, Huang J S, Lai C C, Huang H W, Lin S J and Chueh Y L 2013 *ACS Appl. Mater. Interfaces* **5** 6017
[43] Zhang Y J, Chen X H, Wang Z R, Chen Q L, Liu G, Li Y, Wang P J, Li R W and Miao X S 2019 *IEEE Trans. Electron Dev.* **66** 4710
[44] Mundle R, Carvajal C and Pradhan A K 2016 *Langmuir* **32** 4983
[45] Tominov R V, Vakulov Z E, Avilov V I, Khakhulin D A, Fedotov A A, Zamburg E G, Smirnov V A and Ageev O A 2020 *Nanomaterials* **10** 1007
[46] Qin X Z, Hu J D, Liu H, Xu X, Yang F, Sun B, Zhao Y, Huang M and Zhang Y 2023 *J. Phys. Chem. Lett.* **14** 3039